

## Article

# Adaptive Equivalent Consumption Minimization Strategy for Fuel Cell Buses Based on Driving Style Recognition

Kun He, Dongchen Qin \*, Jiangyi Chen, Tingting Wang, Hongxia Wu and Peizhuo Wang

School of Mechanical and Power Engineering, Zhengzhou University, Zhengzhou 450001, China

\* Correspondence: dcqin@zzu.edu.cn; Tel.: +86-136-2386-8575

**Abstract:** Driving style has a significant effect on the operating economy of fuel cell buses (FCBs). To reduce hydrogen consumption and prolong the fuel cell life of FCBs, this paper proposes an online adaptive equivalent consumption minimum strategy (A-ECMS) based on driving style recognition. Firstly, driving data from various drivers is collected, and a standard driving cycle is created. Neural networks are then used to identify driving conditions, and three fuzzy logic recognizers are developed to identify driving styles for different driving conditions. The driving style factor is associated with the equivalent factor using an optimization algorithm that incorporates hydrogen consumption cost and fuel cell degradation cost into the objective function. Simulation results demonstrate that the proposed A-ECMS can reduce equivalent hydrogen consumption, prolong fuel cell life, and result in a 6.2% reduction in total operating cost compared to the traditional method.

**Keywords:** driving style recognition; equivalent consumption minimization strategy; fuel cell degradation; fuel cell bus



**Citation:** He, K.; Qin, D.; Chen, J.; Wang, T.; Wu, H.; Wang, P. Adaptive Equivalent Consumption Minimization Strategy for Fuel Cell Buses Based on Driving Style Recognition. *Sustainability* **2023**, *15*, 7781. <https://doi.org/10.3390/su15107781>

Academic Editors: Jiankun Peng, Fengyan Yi, Dawei Pi and Yue Wang

Received: 30 March 2023

Revised: 3 May 2023

Accepted: 5 May 2023

Published: 9 May 2023



**Copyright:** © 2023 by the authors. Licensee MDPI, Basel, Switzerland. This article is an open access article distributed under the terms and conditions of the Creative Commons Attribution (CC BY) license (<https://creativecommons.org/licenses/by/4.0/>).

## 1. Introduction

The massive use of fossil fuels has brought climate warming, air pollution, and energy depletion to mankind. Fuel cell electric vehicles (FCEVs) are considered one of the solutions to the current energy crisis because of their high efficiency and zero emissions [1]. Due to the slow dynamic response and soft output characteristics of fuel cells, FCEVs are generally powered by fuel cells and energy storage sources (ESSs) [2]. Lithium-ion batteries have a high energy density and are one of the most widely used ESSs [3]. In the operation of FCEVs, the energy management strategy allocates energy according to the vehicle demand power and the status of different energy sources to achieve the purpose of peak-shaving and valley-filling while maintaining the state of charge (SOC) of the battery, suppressing the power fluctuation of the fuel cell, and reducing the energy consumption, which is one of the key technologies of FCEVs [4]. Many scholarly studies have shown that different driving styles have a significant effect on fuel economy, and driving styles are also influenced by a variety of factors, such as personal characteristics, current physiological and psychological state, weather conditions, and road environment [5], and even the same driver can exhibit different driving styles under different road conditions [6]. Different driving styles can directly affect the energy distribution of the vehicle's powertrain. In order to improve the economy of FCEVs and prolong the fuel cell life, it is crucial to introduce the influence of driving style into the energy management strategy.

Energy management strategies for FCEVs can be classified into three categories: rule-based management strategies, optimization-based management strategies, and learning-based management strategies [7], where rule-based management strategies can be divided into deterministic rules and fuzzy rules, and optimization-based control strategies can be divided into real-time optimization and global optimization.

In practical applications, the rule-based control strategy is the most common energy management strategy for FCEVs, which is based on the experience of designers [8]. Deterministic rule-based management strategies include mainly thermostatic control, power

following, and state machine control [9]. Li et al. [10] proposed a state machine control strategy based on droop control, which avoids fast changes in output power. The control strategies based on fuzzy logic mainly include optimal fuzzy control, predictive fuzzy control, and adaptive fuzzy control. Zhao [11] proposed a fuzzy logic-based energy management strategy for a multi-energy hybrid power system and improved the fuzzy logic with a dynamic planning algorithm to achieve the optimal distribution of output power. In the study of rule-based management strategies, the power of fuel cells will fluctuate greatly when different rules are switched. Most scholars focus on the reduction in vehicle equivalent hydrogen consumption and the maintenance of battery SOC, ignoring the durability problem caused by fuel cell fluctuation.

Learning-based energy management strategies are based on data mining and large data sets to generate optimal power output sequences for fuel cells and ESSs, which have the advantage of being more adaptable and do not require a specialized knowledge base [12]. Wu et al. [13] proposed a reinforcement learning-based energy management strategy for fuel cell hybrid ships to achieve optimal operating costs. The learning-based energy management strategy has good adaptability to different operating conditions, but its drawback is that the quality of the management strategy depends on a large database and also requires a lot of time and resources in the learning process.

The optimization-based energy management strategy minimizes fuel consumption by calculating torque or power [14]. The global optimization strategy is to optimize the solution according to a certain objective function for a known complete operating condition. This strategy can obtain the global optimal solution, but its disadvantage is that the complete operating conditions need to be known in advance [15]. Xu et al. [16] proposed an energy management strategy based on deterministic dynamic programming for plug-in proton exchange membrane fuel cell (PEMFC) vehicles, and the road test results showed that the proposed energy management strategy could reduce 9.5% of the daily operating costs.

Real-time optimization strategies have good practical application prospects because they overcome the limitations of global optimization strategies without the need to know the global operating conditions in advance [17]. Real-time optimization mainly includes equivalent consumption minimization strategy (ECMS) [18], model predictive control [19], decoupling control [20], extreme value search [21], and sliding mode control [22]. Among them, ECMS is the hot spot of research, which was first applied to the energy management of hybrid vehicles, and the main idea is to equate the consumption of battery electric energy to the consumption of fuel. Li et al. [23] introduced battery degradation into the fuel cell energy management strategy and proposed an online ECMS, which was verified by real vehicles, and the whole vehicle hydrogen consumption was reduced by 2.16%.

To demonstrate the effect of a driver's driving style on fuel economy, a large number of studies have been conducted by different scholars [24–26]. Qin et al. [27] proposed a hybrid vehicle control strategy based on driving style identification, which improved the fuel economy of the vehicle. Guo et al. [28] decoupled driving style from driving conditions in order to accurately identify driving style and introduced it into the energy management system of plug-in hybrid electric vehicles, which improved the fuel economy of the vehicles. Offline driving style algorithms [29,30] are more widely used, but there is still a large distance from the online application of vehicles, and in addition, driving style is often described qualitatively; the lack of quantitative representation is not conducive to the application of driving style to the energy management strategy of vehicles.

Based on the above literature review, the limitations of the existing energy management strategies can be summarized as follows:

- (1) In the energy management strategy, different scholars have studied the influence of factors such as vehicle and road conditions [31,32] on the energy management strategy, integrated these influences into the reference range of the energy management strategy, and developed a variety of adaptive energy management strategies, but these methods rarely focus on the influence of the driver on the energy management strategy. This poses a new challenge to the energy management strategy of fuel cell vehicles.

- (2) At the same time, the high cost of fuel cells, the core component of fuel cell buses, has been one of the main factors affecting the promotion of fuel cell buses. The existing energy management strategies focus more on the hydrogen consumption cost and lack consideration of the fuel cell degradation cost [33].

To fill these research gaps, this paper designs an online adaptive equivalent consumption minimum strategy (A-ECMS) based on driving style recognition for fuel cell buses (FCBs). Figure 1 illustrates the structure and main content of the paper, which includes the following contributions:

- (1) In this paper, the influence of driving style is introduced into the FCB energy management strategy, and the parameters in the objective function are adaptively adjusted with the driving style factor to achieve the optimal control effect.
- (2) Multi-objective optimization incorporates equivalent hydrogen consumption and fuel cell degradation into the objective function, improving vehicle economy over the full life cycle.

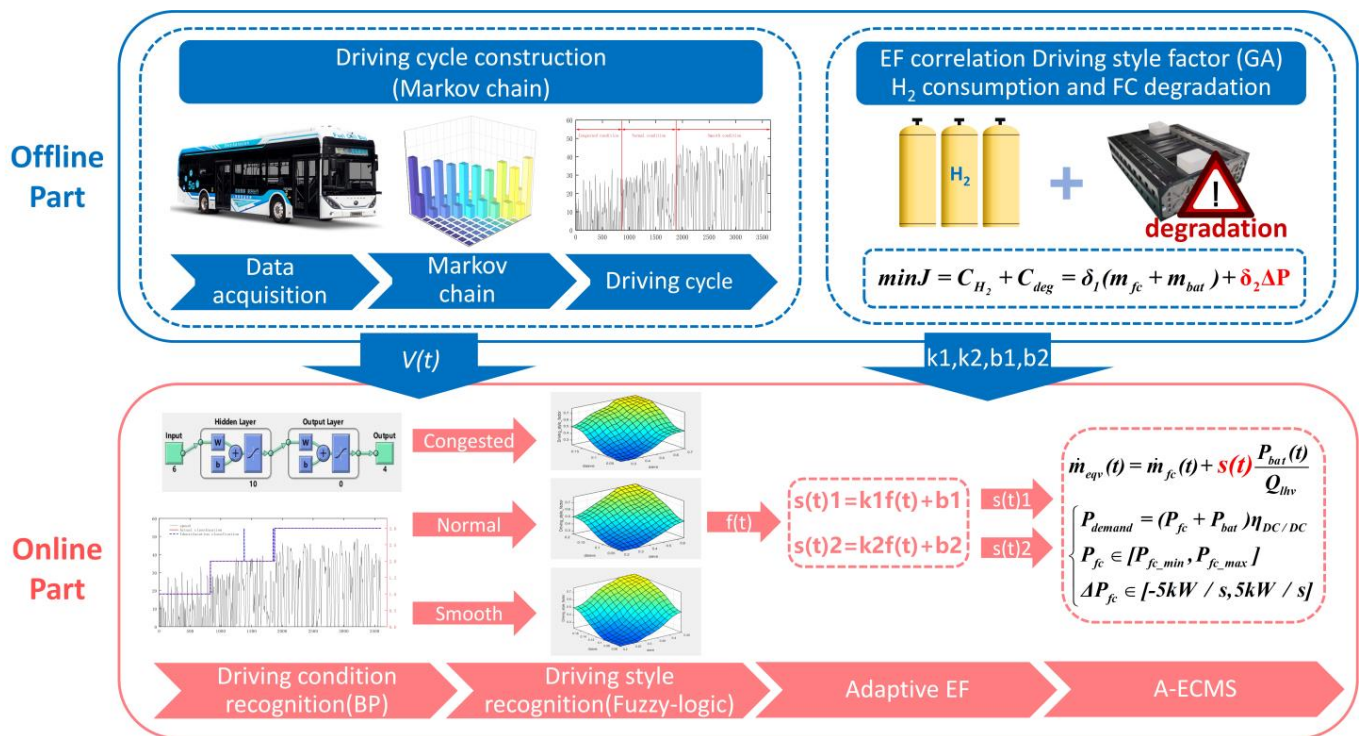


Figure 1. The structure and main contents of the paper.

The structure of this paper is as follows: Section 2 describes the hybrid powertrain model, including the powertrain, fuel cell, battery, and fuel cell degradation model; Section 3 introduces driving data collection and Markov chain-based driving cycle construction; the identification of driving conditions and driving style is in Section 4; Section 5 contains the correlation between the EF and the driving style factor and the comparison of simulation results of various energy management strategies; the conclusions are given in Section 6.

## 2. Hybrid Powertrain Model

### 2.1. Powertrain Architecture

The basic parameters and hybrid powertrain architecture of FCBs are shown in Table 1 and Figure 2. A fuel cell and battery are connected to the DC-bus by unidirectional and bidirectional DC/DC converters, respectively. Energy could be delivered from the battery to the DC-bus, and the DC-bus could also charge the battery when the battery SOC is low.

The DC-bus is connected to the electric motor by a DC/AC converter to provide power to the vehicle.

**Table 1.** Basic parameters of FCBs.

Parameter Name	Parameter Value
Unladen vehicle mass	12,800 kg
Total mass	18,000 kg
Fuel cell stack power	80 kW
Battery capacity	105 kWh
Hydrogen system	8 × 140 L, 35 MPa
Front projection area	7.9 m <sup>2</sup>
Drag coefficient	0.65
Rolling resistance coefficient	0.012

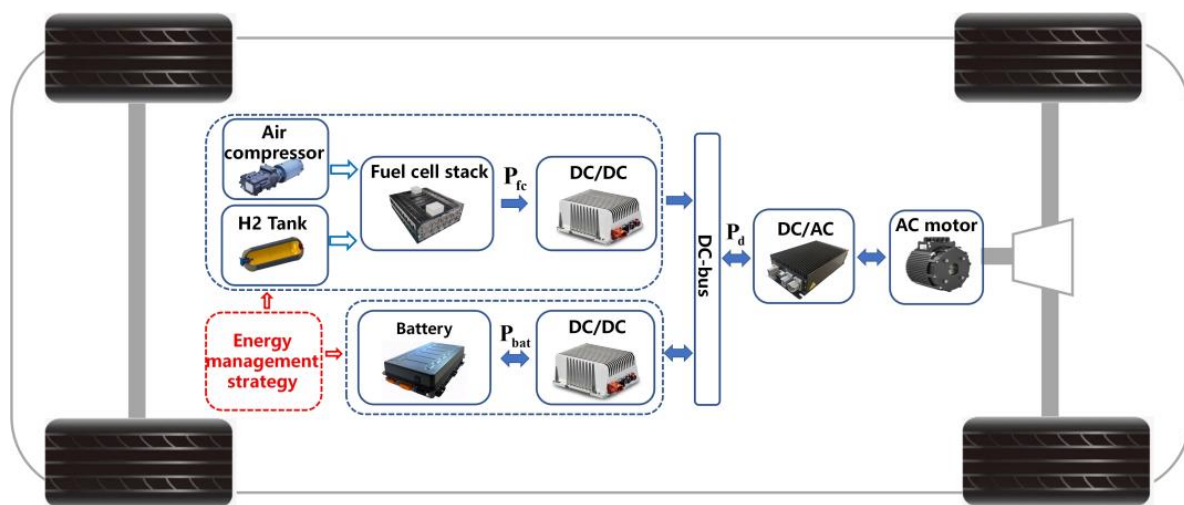


**Figure 2.** Hybrid powertrain architecture.

The on-wheel power demand  $P_{\text{wheels}}$  of the vehicle can be calculated through the longitudinal dynamics of a road vehicle, as shown in Equation (1) [34]:

$$P_{\text{wheels}} = v(mgC_r \cos \theta + mg \sin \theta + \frac{1}{2}C_d A \rho_{\text{air}} v^2 + \delta m \frac{dv}{dt}) \quad (1)$$

where  $v$  is the vehicle speed,  $m$  is the vehicle mass,  $g$  is the acceleration of gravity,  $C_r$  is the rolling resistance coefficient,  $\theta$  is the slope of the road,  $C_d$  is the air resistance coefficient,  $A$  is the front surface area,  $\rho_{\text{air}}$  is the air density, and  $\delta$  is the rotating mass coefficient.

The power demand on the DC-bus  $P_{\text{demand}}$  can be described as Equation (2):

$$P_{\text{demand}} = \frac{P_{\text{wheels}}}{\eta_{\text{DC/AC}} \eta_{\text{motor}}} \quad (2)$$

where  $\eta_{\text{DC/AC}}$  is the efficiency of the DC/AC converter and  $\eta_{\text{motor}}$  is the efficiency of the motor.

The DC-bus is powered by a fuel cell and battery through DC/DC converters, calculated as Equation (3):

$$P_{\text{demand}} = P_{fc} \eta_{\text{DC/DC}} + P_{bat} \eta_{\text{DC/DC}} \quad (3)$$

where  $P_{fc}$  is the fuel cell stack output power,  $P_{bat}$  is the battery output power, and  $\eta_{\text{DC/DC}}$  is the efficiency of the DC/DC converter.

## 2.2. Fuel Cell Model

The PEMFC is the main energy source for an FCB, which converts the chemical energy of hydrogen into electrical energy through an electrochemical reaction. The single fuel cell voltage  $V_{cell}$  can be described as Equation (4) [35]:

$$V_{cell} = E_{nerest} - V_{act} - V_{ohm} - V_{con} \quad (4)$$

where  $E_{nerest}$  is the thermodynamic potential,  $V_{act}$  is the activation losses,  $V_{ohm}$  is the ohmic losses, and  $V_{con}$  is the concentration losses.

The thermodynamic potential  $E_{nerest}$  can be calculated as Equation (5) [36]:

$$E_{nerest} = 1.229 - 0.85e^{-3}(T - T_{ref}) + \frac{RT}{2F} \left[ \ln(p_{H_2}) + \frac{1}{2} \ln(p_{O_2}) \right] \quad (5)$$

where  $T$  is the thermodynamic temperature of the reaction process,  $T_{ref}$  is the temperature correction offset,  $R$  is the gas constant,  $F$  is the Faraday constant, and  $p_{H_2}$  and  $p_{O_2}$  are the partial pressures of hydrogen and oxygen, respectively.

The activation losses  $V_{act}$  can be described as Equation (6) [36]:

$$V_{act} = \zeta_1 + \zeta_2 T + \zeta_3 T \ln C_{O_2} + \zeta_4 \ln I_{st} \quad (6)$$

where  $\zeta_1$ ,  $\zeta_2$ ,  $\zeta_3$  and  $\zeta_4$  are coefficients subject to temperature and pressure, with values of  $-0.9514$ ,  $0.00395$ ,  $0.000074$ , and  $-0.000187$ , respectively.  $C_{O_2}$  is the oxygen concentration in the catalytic layer of the cathode, and  $I_{st}$  is the fuel cell stack current.

The ohmic losses  $V_{ohm}$  are the voltage drop generated by the equivalent internal resistance in the reaction and can be calculated as Equation (7):

$$V_{ohm} = I_{st}(R_M + R_C) \quad (7)$$

where  $R_M$  and  $R_C$  are the resistances of ions passing through the exchange membrane and electrons passing through the electrode.

The concentration losses  $V_{con}$  are expressed as the voltage drop due to the decrease in oxygen and hydrogen concentrations and can be described as Equation (8) [36]:

$$V_{con} = -B \ln \left( 1 - \frac{i}{i_{max}} \right) \quad (8)$$

where  $B$  is a constant depending on the fuel cell type and its operation mode,  $i$  is the actual current density, and  $i_{max}$  is the maximum value of the current density.

The hydrogen consumption rate can be calculated as Equation (9) [37]:

$$\dot{m}_{H_2} = \frac{NM_{H_2}}{nF} I_{st} \quad (9)$$

where  $N$  is the number of stack cells,  $M_{H_2}$  is the molar mass of hydrogen, and  $n$  is the number of charges transferred per mole of hydrogen.

The hydrogen filling price at hydrogen refueling stations is 4 USD/kg [38], so the hydrogen cost factor  $\delta_1$  is taken as 4 USD/kg, and the hydrogen consumption cost can be described as Equation (10):

$$C_{H_2} = \delta_1(m_{fc} + m_{bat}) = \delta_1 \left( m_{fc} + \frac{\int P_{bat}(t)}{Q_{lhv}} \right) \quad (10)$$

where  $m_{fc}$  and  $m_{bat}$  denote the fuel cell hydrogen consumption and the battery equivalent hydrogen consumption, respectively, and  $Q_{lhv}$  is the hydrogen low heating value.

The fuel cell stack power  $P_{stack}$  can be described as Equation (11):

$$P_{stack} = NV_{cell}I_{st} \quad (11)$$

The output power  $P_{fc}$  can be calculated as Equation (12):

$$P_{fc} = P_{stack} - P_{aux} \quad (12)$$

where  $P_{aux}$  is the auxiliary system power.

The fuel cell efficiency  $\eta_{fc}$  can be described as Equation (13):

$$\eta_{fc} = \frac{P_{fc}}{\dot{m}_{H_2}Q_{lhv}} \quad (13)$$

### 2.3. Battery Model

In the hybrid powertrain architecture, the battery is used as an auxiliary power source to provide energy to the DC-bus, and the classical R-int model is used for battery modeling [39]. In the model, the current of the battery  $I_{bat}$  can be described as Equation (14):

$$I_{bat} = \frac{V_{oc} - \sqrt{V_{oc}^2 - 4R_{bat}P_{bat}}}{2R_{bat}} \quad (14)$$

where  $V_{oc}$  and  $R_{bat}$  denote the open-circuit voltage and equivalent internal resistance of the battery, respectively, which are functions of the battery SOC, and  $P_{bat}$  is the battery output power.

The instantaneous SOC(t) of the battery can be calculated as Equation (15):

$$SOC(t) = SOC(0) - \int \frac{I_{bat}}{Q_{bat}} dt \quad (15)$$

where SOC(0) is the initial SOC and  $Q_{bat}$  is the battery capacity.

### 2.4. Fuel Cell Degradation Cost Model

A fuel cell power stack is the main power source of hybrid power systems, and it will inevitably degrade due to changes in output power [40]. In order to analyze the effect of energy management strategies on the degradation of the stack, a fuel cell degradation cost model is constructed.

The degradation cost of the fuel cell can be calculated as Equation (16):

$$C_{deg} = \delta_2 \Delta P \quad (16)$$

where  $\delta_2$  is the fuel cell degradation cost factor per percentage and  $\Delta P$  is the fuel cell degradation rate.

The degradation of a fuel cell is primarily caused by load change cycles, start-stop cycles, idle conditions, and high power load conditions. Based on experimental data from the literature [41], the degradation rate for each load change cycle is 0.593 ppm, the degradation rate for each start-stop cycle is 19.6 ppm, in idle conditions, each hour of idle operation results in a degradation rate of 12.6 ppm, and for high power load conditions, the degradation rate is 14.7 ppm per hour. The degradation of the fuel cell  $\Delta P$  caused by the four operating conditions can be described as Equation (17):

$$\Delta P = P_1 N_1 + P_2 N_2 + P_3 T_1 + P_4 T_2 \quad (17)$$

where  $N_1$  and  $N_2$  represent the number of load change cycles and start-stop cycles, respectively, and  $T_1$  and  $T_2$  represent the idle condition time and high power load condition time, respectively.

Defining a fuel cell degradation rate of 10% as failure, the fuel cell unit degradation cost factor  $\delta_2$  can be calculated as Equation (18):

$$\delta_2 = \frac{\gamma_{stack} P_{fc\_rated}}{10} \quad (18)$$

where  $\gamma_{stack}$  denotes the unit cost of the stack (117 USD/kW) [42], and  $P_{fc\_rated}$  is the rated power of the stack.

### 3. Data Acquisition and Driving Cycle Construction

#### 3.1. Data Acquisition and Pre-Processing

The driving cycle is the time-speed profile of the vehicle. In order to provide a basis for the optimization and simulation of the energy management strategy, it is necessary to construct a driving cycle that meets the operating characteristics of the FCBs. Before the simulation started, the driving data of 10 drivers on the same bus line were collected using GPS terminals. The driving data collection vehicle is a 12 m class FCB, which matches the modeled vehicle, and the bus line is selected as Bus Rapid Transit (BRT) B18 of Zhengzhou Bus Group, and the route is shown in Figure 3. The line is 19.9 km long with 36 bus stops, extending from the northwest to the center of the city and covering a wide range of road types, including suburban roads, BRT, and congestion-prone urban roads. The 10 drivers, including 8 men and 2 women, had an average age of 45 and an average driving experience of 18.5 years. To account for variability in pedestrian flow conditions, data collection was conducted seven days a week, including Monday through Sunday. The data duration reached 37,180 s, with a sampling time of 1 s.

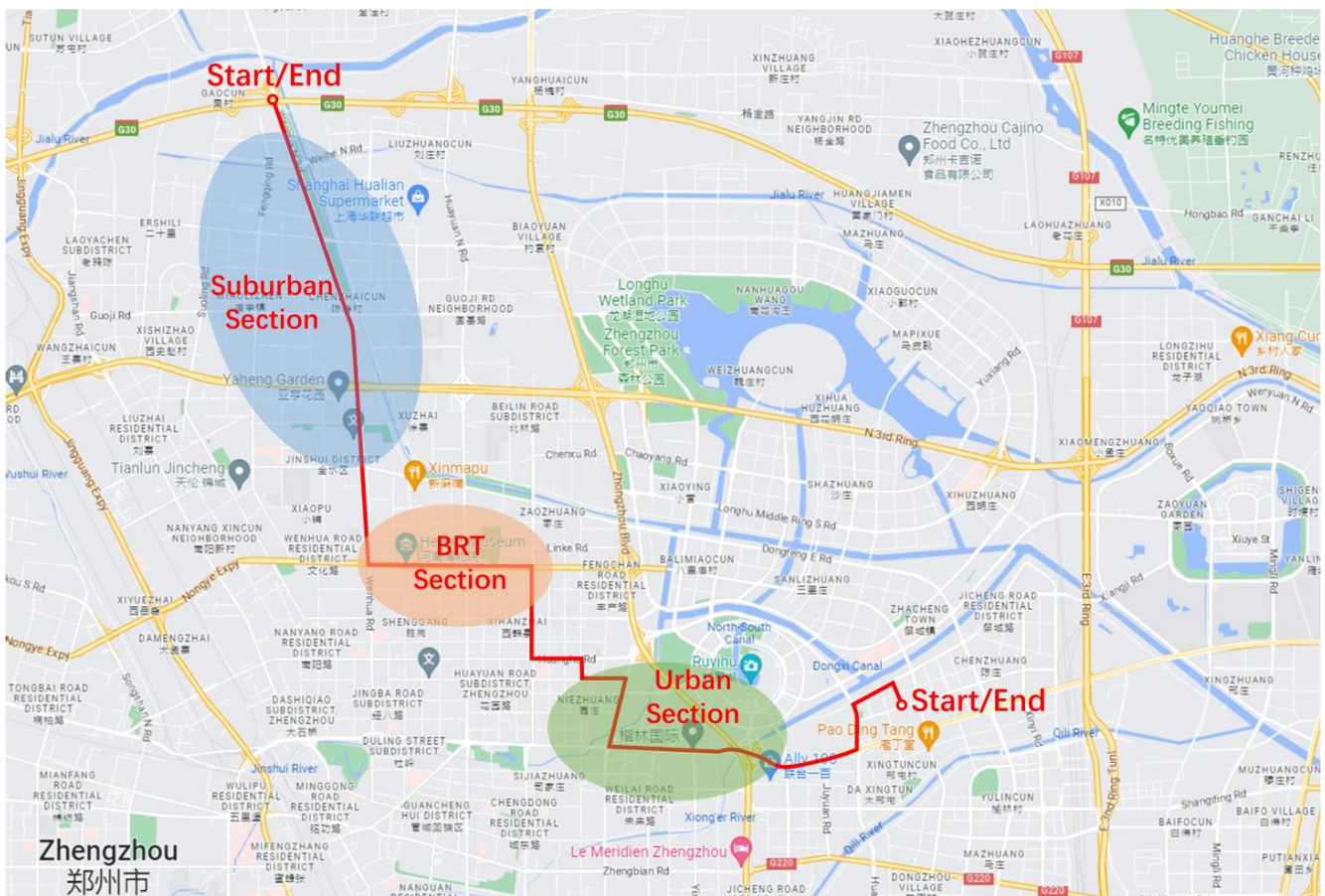


Figure 3. Bus route map.

Due to the interference in the acquisition process, there are missing and abnormal data that cannot be directly used for the construction of the driving cycle, and the data need to be pre-processed. For missing data points, if the speed before and after the missing point is 0, the vehicle is defined as being in a non-running state, and the missing data will be filled as 0. If the speed before and after the missing point is not 0, the interpolation algorithm is used for the known speed segment to generate reasonable speed values for filling. For abnormal data, such as acceleration and deceleration beyond probable values and abnormal data due to force majeure, the data are eliminated to ensure the reasonableness of the driving cycle data [28].

### 3.2. Principal Component Analysis and Cluster Analysis

To construct the driving cycle, the pre-processed data are first divided into 477 kinematic segments based on the complete kinematic segment principle, which involves starting from the idle phase, going through the acceleration, uniform speed, and deceleration phases, and entering the idle phase again. To describe the characteristics of these segments, 10 parameters are reported in Table 2.

**Table 2.** Characteristic parameters.

Parameter	Unit	Description
$\bar{v}$	m/s	Average velocity
$v_{max}$	m/s	Maximum velocity
$a_{max}$	m/s <sup>2</sup>	Maximum acceleration
$a_{min}$	m/s <sup>2</sup>	Minimum acceleration
$P_l$	%	Time ratio of low-speed (0–10 km/h)
$P_m$	%	Time ratio of medium-speed (10–25 km/h)
$P_h$	%	Time ratio of high-speed (above 25 km/h)
$P_i$	%	Time ratio of idling
$P_a$	%	Time ratio of acceleration
$P_d$	%	Time ratio of deceleration

The matrix of characteristic parameters of the kinematic segments is in Table 3. When kinematic segments are described using characteristic parameters, direct cluster analysis may lead to distorted results due to the large number of characteristic parameters and their possible correlation with each other. The principal component analysis (PCA) method can transform the feature parameters with correlation into mutually independent feature parameters and thus improve the calculation speed. Using the PCA method, the steps of data standardization, covariance matrix calculation, and correlation test of the characteristic parameter matrix are completed in turn, and the first four components are selected as the principal components of the kinematic segments from the calculated principal components. Their cumulative contribution rate reached 92.15%, which exceeded the limit of 85% [43].

In the clustering algorithm, the position of the initial center of mass can largely affect the clustering results. Traditional K-means has randomness in the selection of the center of mass, and this randomness may lead to slow convergence of the algorithm. The K-means++ clustering algorithm is improved in the initialization process of the center of mass so that the initial centers of mass are as far away from each other as possible, which can avoid the above problem. In the clustering, the four principal components are used as the analysis factors, and the K-means++ algorithm is used to divide the 477 kinematic segments into three classes. The first class sample of 111 segments with an average speed of 7 km/h and 75% of the low speed ratio can be represented as the congested condition. The second class sample of 137 segments with an average speed of 13.74 km/h, 42% of the low speed ratio, and 39% of the medium speed ratio can be represented as the normal condition. The third class sample of 230 segments with an average speed of 22.67 km/h, 29% of the low speed ratio, 20% of the medium speed ratio, and 51% of the high speed ratio can be expressed as

the smooth condition. The percentages of the three types of driving conditions are 23%, 29%, and 48%, respectively.

**Table 3.** Matrix of characteristic parameters.

Segment	$\bar{v}$	$v_{max}$	$a_{max}$	$a_{min}$	$P_l$	$P_m$	$P_h$	$P_i$	$P_a$	$P_d$
1	16.26	29.61	0.65	−0.83	0.26	0.63	0.12	0.07	0.47	0.49
2	16.31	35.17	1.09	−1.05	0.27	0.55	0.18	0.10	0.47	0.43
3	10.44	22.28	1.24	−1.18	0.52	0.48	0.00	0.29	0.29	0.48
4	17.92	40.33	1.02	−0.75	0.40	0.24	0.36	0.11	0.44	0.47
5	12.66	32.36	1.02	−1.19	0.45	0.33	0.21	0.27	0.35	0.40
6	13.12	28.20	1.19	−1.12	0.38	0.47	0.15	0.26	0.41	0.35
...	...	...	...	...	...	...	...	...	...	...
...	...	...	...	...	...	...	...	...	...	...
472	23.26	46.48	1.81	−1.28	0.23	0.27	0.50	0.17	0.43	0.42
473	19.69	41.09	0.90	−0.92	0.38	0.20	0.43	0.20	0.46	0.36
474	21.14	43.56	1.58	−1.41	0.25	0.34	0.41	0.06	0.39	0.56
475	28.88	48.33	1.49	−1.68	0.21	0.14	0.65	0.07	0.38	0.56
476	22.07	48.35	1.21	−1.51	0.40	0.13	0.47	0.22	0.44	0.36
477	28.26	45.12	1.94	−1.03	0.22	0.16	0.62	0.10	0.44	0.48

### 3.3. Markov Chain-Based Driving Cycle Construction

The driving process of a FCB satisfies no memory or randomness, which is a typical Markov process. In the driving cycle construction, the time-speed variation is transformed into time-state variation, the transfer frequency of adjacent states is counted, and the frequency is converted into probability by maximum likelihood estimation to construct the state transfer probability matrix [44].

Steps in the driving cycle's construction:

- (1) Set the initial driving state to 1, and determine the state value of the next moment from the state transfer probability matrix.
- (2) Based on Markov chain theory, the state sequence is transformed into a velocity sequence by Equation (19).

$$v_t = (S_t - 1 + r_d)\Delta d \quad (19)$$

where  $v_t$  denotes the instantaneous velocity value,  $S_t$  denotes the instantaneous state value,  $r_d$  is a random number with the value range  $[0, 1]$ , and  $\Delta d$  denotes the velocity interval of the state.

- (3) Calculate the characteristic parameters of the speed sequence and compare them with the actual driving cycle values to determine whether the absolute deviation value does not exceed 10%.

According to the results of the cluster analysis and the operation characteristics of FCBs, a 3600-s driving cycle was constructed, as shown in Figure 4. The working conditions include 830 s of congestion, 1033 s of normal operation, and 1737 s of smooth operation, with average speeds of 7 km/h, 13.74 km/h, and 22.67 km/h, respectively, and maximum speeds of 30 km/h, 40 km/h, and 50 km/h, respectively.

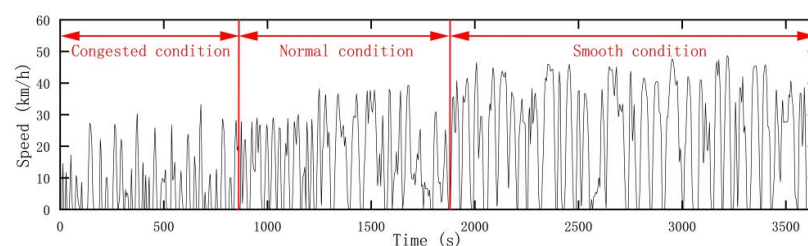


**Figure 4.** Driving cycle over 3600 s.

#### 4. Driving Conditions and Driving Style Recognition

An aggressive driver driving a vehicle in smooth conditions may appear calm in terms of acceleration and acceleration rate of change, while an economical driver operating the gas and brake pedals in congested road conditions may appear more aggressive, so decoupling driving style from driving conditions is necessary to accurately identify driving style [30].

##### 4.1. Driving Condition Recognition Using an Artificial Neural Network

The recognition of driving conditions mainly includes clustering algorithm recognition [26], fuzzy logic recognition, and neural network recognition. The clustering algorithm recognition is dependent on the initial clustering center, while the recognition of fuzzy logic is largely influenced by human factors, and the neural network recognition avoids the defects of the above two ways while having a higher recognition accuracy.

The backpropagation (BP) neural network consists of an input layer, a hidden layer, and an output layer. In driving condition recognition, the input layer consists of 10 characteristic parameters of driving data, while the output layer represents the three driving conditions. The number of neurons in the hidden layer is set to 10 using an empirical formula, resulting in a network structure of 10-10-3. The training function used is the Trainlm function.

The driving cycle constructed based on the Markov chain is imported into the neural network model for recognition. The results show that the constructed recognizer can identify the current driving conditions very well, as shown in Figure 5.

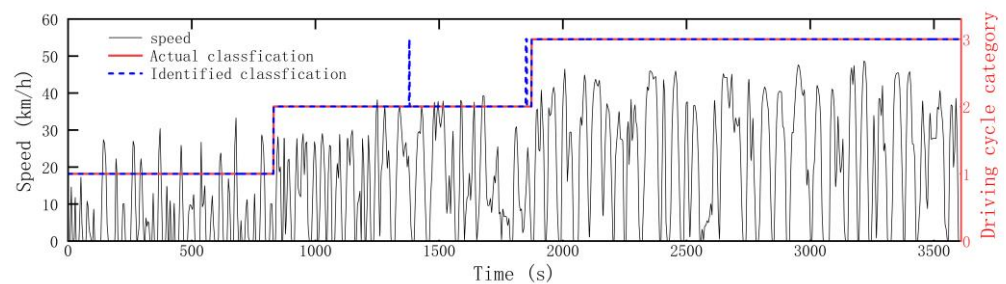


**Figure 5.** Driving condition recognition result.

##### 4.2. Driving Style Recognition Based on Fuzzy Logic

Different driving styles can be broadly classified into three types: Aggressive (A), Ordinary (O), and Economical (E). Identifying driving styles is a subjective process that depends on human experience and knowledge and cannot be represented by rigorous mathematical expressions [30]. Therefore, using fuzzy logic to identify driving styles has inherent advantages.

To decouple driving style from driving conditions, three fuzzy logic controllers are constructed for three driving conditions: congested, normal, and smooth. Each controller uses the average acceleration and rate of change of the average acceleration within a 120-s interval as inputs and outputs a driving style factor with a value range of (0, 1), where a value close to 1 indicates a more aggressive driving style and a value close to 0 indicates a more economical driving style. The membership functions are chosen to take into account the effect of driving cycles on driving style. The membership functions and fuzzy rules are shown in Tables 4–6.

**Table 4.** Average acceleration membership function for three driving conditions.

	L(zmf)	M(gaussmf)	H(smf)
<b>Congested</b>	[0.25, 0.4]	[0.45, 0.33]	[0.26, 0.4]
<b>Normal</b>	[0.26, 0.54]	[0.1, 0.42]	[0.3, 0.56]
<b>Smooth</b>	[0.34, 0.58]	[0.1, 0.5]	[0.5, 0.6]

**Table 5.** Average acceleration rate of the change membership function for three driving conditions.

	L(zmf)	M(gaussmf)	H(smfm)
<b>Congested</b>	[0.09, 0.15]	[0.22, 0.12]	[0.1, 0.15]
<b>Normal</b>	[0.06, 0.16]	[0.03, 0.112]	[0.07, 0.17]
<b>Smooth</b>	[0.07, 0.14]	[0.02, 0.11]	[0.08, 0.14]

**Table 6.** Fuzzy rules.

Average Acceleration	Average Acceleration Rate of Change		
	L	M	H
L	E	E	O
M	E	O	A
H	O	A	A

## 5. A-ECMS Based on Driving Style

### 5.1. ECMS

The ECMS is a control strategy for real-time optimization based on the Pontryagin Minimal Principle (PMP), which was proposed by Pontryagin et al. [45]. Its objective is to minimize hydrogen consumption by allocating the output power of the fuel cell and battery. This approach allows for an approximate global optimal solution to be obtained with guaranteed computational speed. The objective can be described as Equation (20):

$$m_{eqv}(t) = m_{fc}(t) + s(t)m_{bat}(t) = m_{fc}(t) + s(t) \frac{P_{bat}(t)}{Q_{lhw}} \quad (20)$$

$$\begin{cases} P_{fc} \in [P_{fc\_min}, P_{fc\_max}] \\ P_{bat} \in [P_{bat\_min}, P_{bat\_max}] \\ \Delta P_{fc} \in [-5kW/s, 5kW/s] \end{cases}$$

where  $s(t)$  is the equivalent factor (EF), which equates the consumption of battery electricity to the consumption of hydrogen.

In order to maintain the battery SOC and ensure efficient fuel cell operation, penalty functions are added to the objective function as Equation (21) [19]:

$$m_{eqv}(t) = K_{fc}m_{fc}(t) + K_{bat}s(t) \frac{P_{bat}(t)}{Q_{lhw}} \quad (21)$$

where  $K_{fc}$  denotes the fuel cell high-efficiency operation penalty function, which can be expressed as Equation (22):

$$K_{fc} = \begin{cases} \left(1 - 2 \frac{\eta - \eta_{opt}}{\eta_{max} - \eta_{min}}\right)^2 & \eta \geq 0.45 \\ \left(1 - 2 \frac{\eta - \eta_{opt}}{\eta_{max} - \eta_{min}}\right)^4 & \eta < 0.45 \end{cases} \quad (22)$$

where  $\eta$  is the instantaneous efficiency of fuel cell operation,  $\eta_{opt}$  is the optimal efficiency (0.48),  $\eta_{max}$  is the maximum efficiency (0.48), and  $\eta_{min}$  is the minimum efficiency (0). When the instantaneous efficiency of the fuel cell  $\eta$  is less than 0.45, the value in the penalty function will become larger, and the output power of the fuel cell will be limited, so as to keep the fuel cell operating in the high efficiency range as much as possible.

$K_{bat}$  denotes the battery SOC maintenance penalty function, which can be expressed as Equation (23):

$$K_{bat} = \begin{cases} \left(1 - \frac{2(SOC(t) - SOC_{opt})}{SOC_{high} - SOC_{low}}\right)^4 & SOC_{low} \leq SOC(t) \leq SOC_{high} \\ \left(1 - \frac{2(SOC(t) - SOC_{opt})}{SOC_{high} - SOC_{low}}\right)^{20} & SOC(t) < SOC_{low}, SOC(t) > SOC_{high} \end{cases} \quad (23)$$

where  $SOC_{opt}$  is the ideal SOC of the battery (0.6),  $SOC_{high}$  and  $SOC_{low}$  are the maximum and minimum values of SOC, which take the values of 0.9 and 0.4, respectively. When the battery SOC is less than 0.4, the penalty function will limit the battery discharge, and when the battery SOC is greater than 0.9, the penalty function will increase the battery discharge power as a way to keep the battery SOC close to the ideal SOC.

### 5.2. EF Adaption Based on Driving Style Factor Using Multi-Objective Optimization

In ECMS, the choice of the EF directly impacts the power distribution of the energy management strategy, making it crucial to establish a correlation between the EF and the driving style factor. The relationship between the EF and the driving style factor can be expressed as Equation (24) [28]. When the battery is in a discharged state and the driving style factor increases, it indicates a greater fluctuation in the vehicle's current power demand. To limit the fluctuation of the fuel cell output power, the EF should be adjusted to a smaller value to increase the battery discharge power. Conversely, when the driving style factor is small, indicating less fluctuation in the driver's power demand, the EF can be adjusted to a larger value to appropriately increase the fuel cell output power.

$$\begin{cases} s_{dis}(t) = k_1 f(t) + b_1 \\ s_{chg}(t) = k_2 f(t) + b_2 \end{cases} \quad (24)$$

where  $s_{dis}(t)$  and  $s_{chg}(t)$  denote the EF when the battery is in charging and discharging states, respectively, and  $f(t)$  denotes the current driving style factor.

In the energy management strategy, both hydrogen consumption and fuel cell degradation affect the overall cost of the vehicle. To improve vehicle efficiency, the optimization algorithm integrates both hydrogen consumption and fuel cell degradation into the objective function. In order to convert the multi-objective problem into a single-objective problem for solution, hydrogen consumption and fuel cell degradation are translated into vehicle operating costs. The multi-objective function is expressed as Equation (25):

$$\min J = C_{H_2} + C_{deg} = \delta_1(m_{fc} + m_{bat}) + \delta_2 \Delta P \quad (25)$$

The optimization process is performed using a genetic algorithm in combination with the Simulink program. The initial population size is set to 50, the iteration limit is set to 100, the crossover probability is set to 0.6, and the variation probability is set to 0.001. The relationship between the EF and the driving style factor is obtained as Equation (26):

$$\begin{cases} s_{dis}(t) = -0.45f(t) + 2.9 \\ s_{chg}(t) = 0.54f(t) + 2.5 \end{cases} \quad (26)$$

### 5.3. Simulation Verification

Based on the above research, the hybrid power system model and driving style-based energy management strategy are simulated and verified using the Matlab/Simulink platform. State machine-based and Fuzzy logic-based control strategies are also constructed for comparison and analysis. Based on the above study, the proposed energy management strategy was evaluated, and the fuel cell output power and battery SOC changes are shown in Figure 6. The results demonstrate that the proposed A-ECMS can meet the power demand of the vehicle under various driving conditions. Furthermore, the A-ECMS performs well in suppressing fuel cell output power fluctuations and maintaining battery SOC.

Figure 7 illustrates the fuel cell output power distribution and efficiency range of four energy management strategies. The proposed A-ECMS fuel cell high efficiency operating range accounted for 87.1% with an average output power of 15.48 kW. In the ECMS, the percentage of the high-efficiency operation interval is 76.18%. The State machine-based and Fuzzy logic-based control strategies exhibit a concentration of output power below 10 kW, with only 42.41% and 46.78% of the high efficiency range, respectively, and their

average output power is 14.57 kW and 13.77 kW, respectively. These results suggest that the introduction of the output power penalty function and driving style factor had a positive effect on improving the fuel cell's output efficiency.

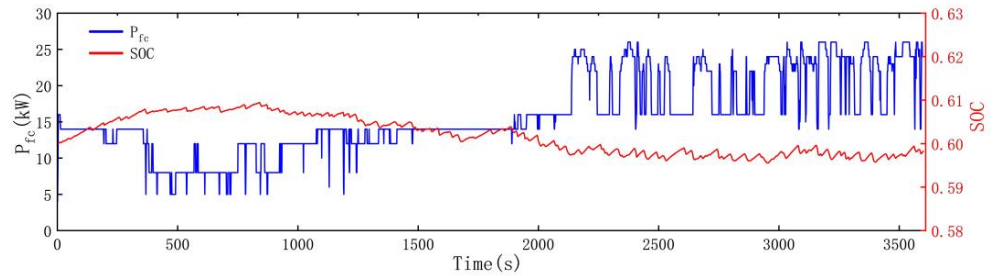


Figure 6. Performance of the A-ECMS on fuel cell power and battery SOC maintenance.

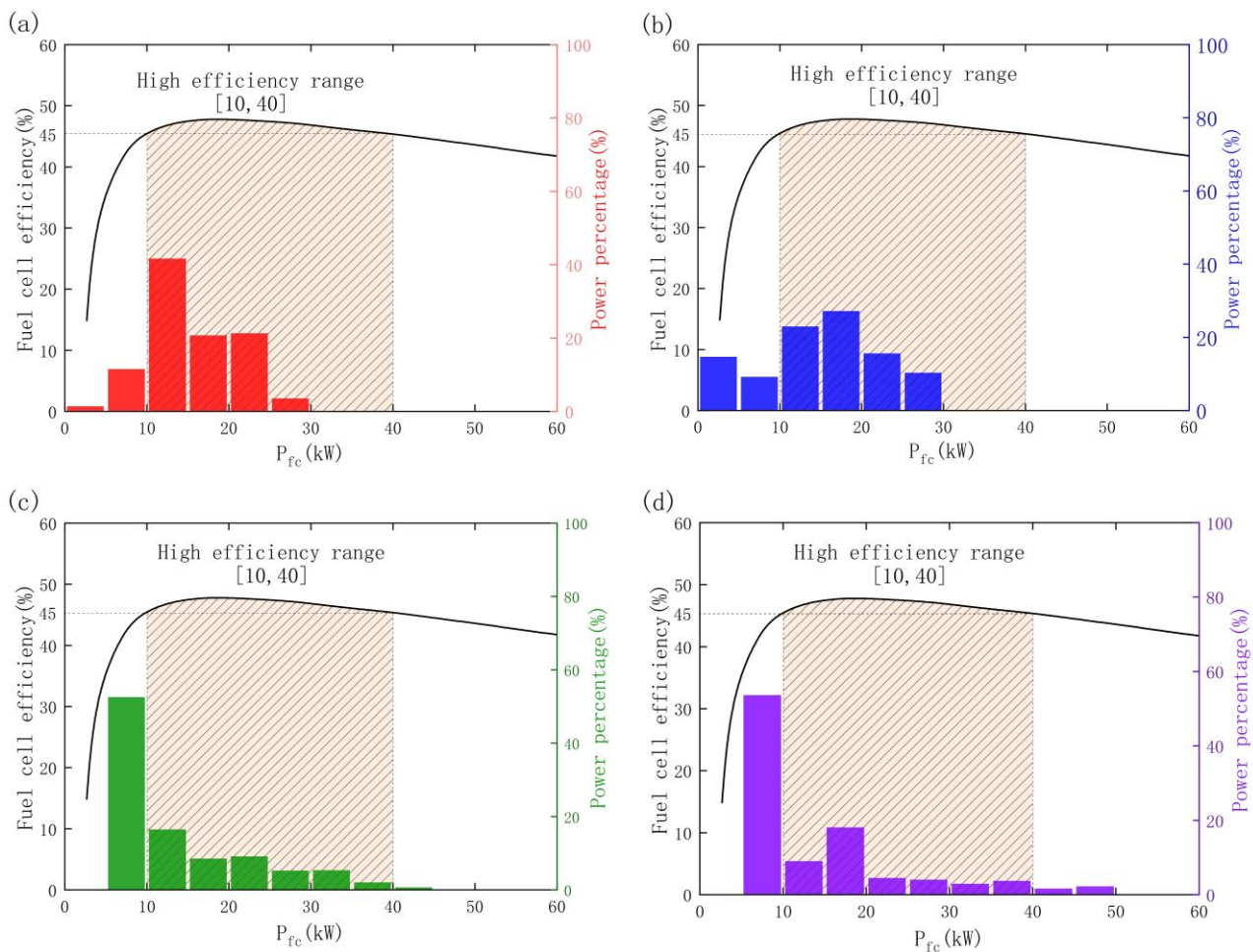
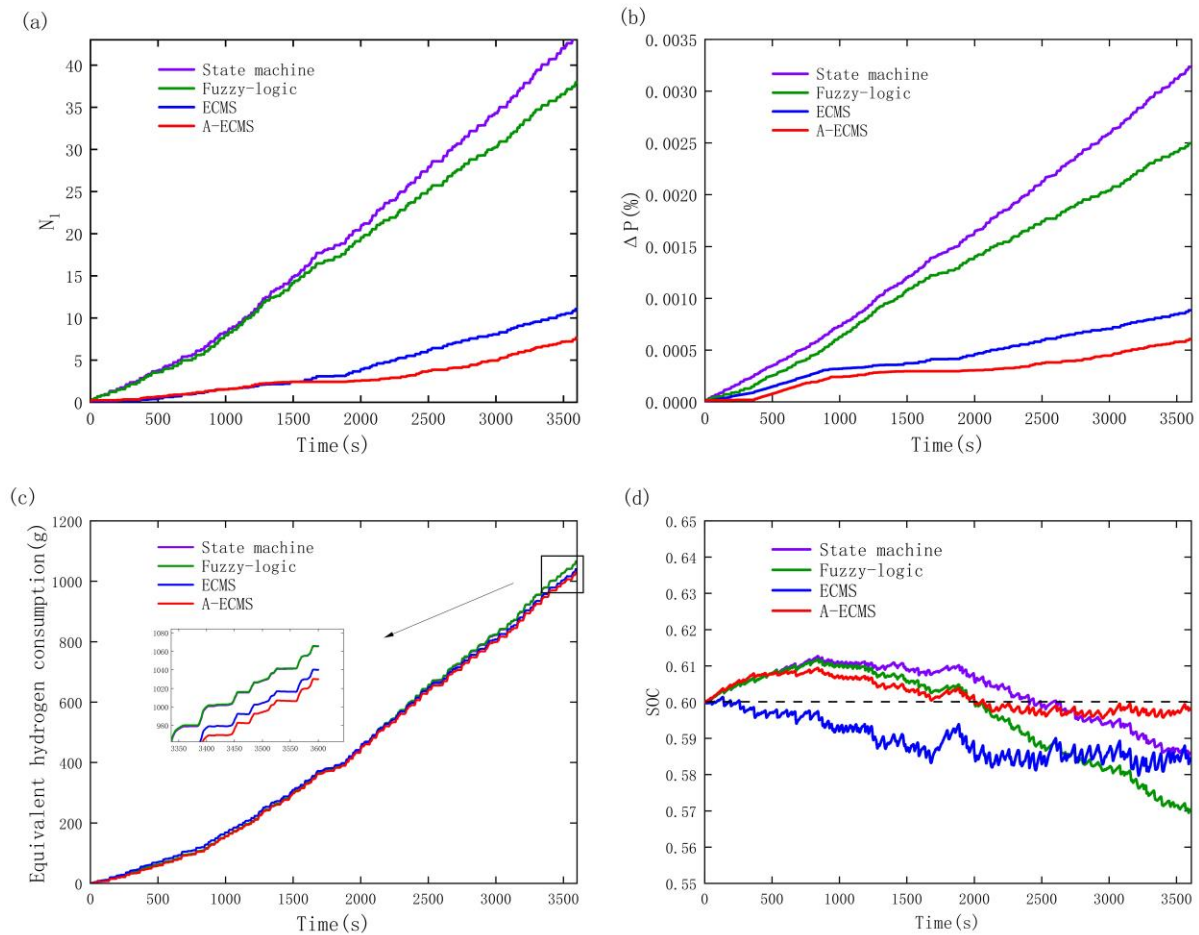


Figure 7. Fuel cell power distribution under different energy management strategies: (a) A-ECMS; (b) ECMS; (c) Fuzzy-logic; (d) State machine.

The fluctuation of fuel cell output power is a significant factor in fuel cell degradation, as shown in Figure 8a, where the power fluctuation of the four energy management strategies is depicted. The State machine-based and Fuzzy logic-based control strategies have larger fuel cell output power fluctuations, with 43.7 and 37.9 load change cycles in the 3600-s driving cycle, respectively. In contrast, due to the introduction of the output power fluctuation limit, the number of load change cycles in the ECMS decreased to 11.06. Moreover, the A-ECMS, which considers driving style, further reduces the fuel cell

output power fluctuation with only 7.66 load change cycles. These results indicate that the introduction of a driving style can further reduce fuel cell output power fluctuations and prolong fuel cell life.



**Figure 8.** Performance of different energy management strategies on (a) number of fluctuating cycles, (b) fuel cell degradation, (c) equivalent hydrogen consumption, and (d) battery SOC maintenance.

By considering the load change cycle, start-stop cycle, large load condition, and idling condition together, the fuel cell degradation curves under the operation of the four energy management strategies are obtained, as shown in Figure 8b. The ECMS can delay fuel cell degradation to a greater extent than the first two energy management strategies, and the simulation results show that the degradation degree is further reduced in the A-ECMS after considering the driving style.

Equivalent hydrogen consumption is an essential indicator of energy management strategies, as depicted in Figure 8c, where the energy consumption of the battery is converted into hydrogen consumption. The real-time optimization algorithm ECMS reduces the equivalent hydrogen consumption by 2.3% and 2.4% compared to the State machine and Fuzzy logic, respectively. Furthermore, after introducing the effect of driving style, the equivalent hydrogen consumption is reduced by another 1% compared to ECMS, indicating that the EF of adaptive adjustment has a positive effect on reducing equivalent hydrogen consumption.

Maintaining the battery SOC within a reasonable interval is an essential part of the energy management strategy. The change in battery SOC of the four energy management strategies is shown in Figure 8d, where A-ECMS performs the best in this regard, with very little change in the initial and end moments of simulation SOC. The battery SOC at the end of ECMS and State machine decreases by 0.015. The Fuzzy logic-based energy management

strategy performs the worst in SOC maintenance, with the battery SOC decreasing from 0.6 to 0.57. This is due to the lower average output power of the fuel cell under the Fuzzy logic control strategy, and the battery consumes more energy under cycling conditions, which in turn leads to a decrease in SOC.

Table 7 presents the performance comparison of the four energy management strategies in terms of fuel cell degradation cost, hydrogen consumption cost, and total operating cost. It shows that ECMS can effectively mitigate fuel cell fluctuations and reduce fuel cell degradation, and the total operating cost decreases by 31.6% and 24.4% compared to the State machine and Fuzzy logic control strategies, respectively. The A-ECMS, which takes into account the influence of the driver's driving style on the energy management strategy, further improves the fuel cell fluctuation suppression and reduces equivalent hydrogen consumption, resulting in a 6.2% reduction in total operating cost compared to the ECMS.

**Table 7.** Costs of different energy management strategies.

Compared to	Degradation Cost (USD)	Hydrogen Consumption Cost (USD)	Total Operating Cost (USD)
State machine	3.03	4.26	7.29
Fuzzy-logic	2.34	4.26	6.6
ECMS	0.83	4.16	4.99
A-ECMS	0.57	4.11	4.68

## 6. Conclusions

This paper proposes a novel A-ECMS for FCBs that incorporates the influence of driving style on the energy management strategy. To accurately identify the driving style, the paper decouples it from driving conditions, and different identification parameters are applied to identify the driving style for different driving conditions. The offline optimization algorithm correlates the EF and the driving style factor to achieve EF adaptation; at the same time, the hydrogen consumption cost and degradation cost due to fuel cell output power change are jointly incorporated into the objective function. Under the constructed driving cycle simulation, 87.13% of the proposed A-ECMS fuel cell output power is in the high efficiency region, and the lithium battery SOC is reduced by only 0.015. The number of fuel cell output power fluctuation cycles is reduced by 30%, and the fuel cell life decay is reduced by 18% compared to ECMS. The above study is based on computer simulations and lacks experimental validation for comparison, and future work should focus on testbed construction and physical validation.

**Author Contributions:** Conceptualization, K.H.; Data curation, D.Q.; Formal analysis, K.H.; Funding acquisition, J.C.; Investigation, H.W.; Methodology, D.Q.; Project administration, D.Q.; Resources, P.W.; Software, K.H.; Supervision, J.C.; Validation, D.Q., J.C. and T.W.; Visualization, K.H.; Writing—original draft, K.H.; Writing—review & editing, D.Q. All authors have read and agreed to the published version of the manuscript.

**Funding:** This research was funded by “Fuel Cell Vehicle and Key Components Technology Research and Demonstration Application” (221100240200) of Henan Provincial Key Science and Technology Special Project in 2022.

**Institutional Review Board Statement:** Not applicable.

**Informed Consent Statement:** Not applicable.

**Data Availability Statement:** Not applicable.

**Acknowledgments:** Thank you to all reviewers for their suggestions to make this paper better.

**Conflicts of Interest:** The authors declare no conflict of interest.

## References

1. Zhou, J.; Feng, C.; Su, Q.; Jiang, S.; Fan, Z.; Ruan, J.; Sun, S.; Hu, L. The Multi-Objective Optimization of Powertrain Design and Energy Management Strategy for Fuel Cell–Battery Electric Vehicle. *Sustainability* **2022**, *14*, 6320. [[CrossRef](#)]
2. Jia, C.; Zhou, J.; He, H.; Li, J.; Wei, Z.; Li, K.; Shi, M. A novel energy management strategy for hybrid electric bus with fuel cell health and battery thermal- and health-constrained awareness. *Energy* **2023**, *271*, 127105. [[CrossRef](#)]
3. Yao, D.; Lu, X.; Chao, X.; Zhang, Y.; Shen, J.; Zeng, F.; Zhang, Z.; Wu, F. Adaptive Equivalent Fuel Consumption Minimization Based Energy Management Strategy for Extended-Range Electric Vehicle. *Sustainability* **2023**, *15*, 4607. [[CrossRef](#)]
4. Ferahtia, S.; Rezk, H.; Ghoniem, R.M.; Fathy, A.; Alkanhel, R.; Ghonem, M.M. Optimal Energy Management for Hydrogen Economy in a Hybrid Electric Vehicle. *Sustainability* **2023**, *15*, 3267. [[CrossRef](#)]
5. Sagberg, F.; Selpi; Bianchi Piccinini, G.F.; Engström, J. A review of research on driving styles and road safety. *Hum. Factors* **2015**, *57*, 1248–1275. [[CrossRef](#)]
6. Wang, R.; Lukic, S.M. Review of driving conditions prediction and driving style recognition based control algorithms for Hybrid Electric Vehicles. In Proceedings of the 2011 IEEE Vehicle Power and Propulsion Conference, Chicago, IL, USA, 6–9 September 2011; pp. 1–7.
7. Manzie, C.; Grondin, O.; Sciarretta, A.; Zito, G. ECMS Controller Robustness in Flex-Fuel Hybrid Vehicles. *J. Dyn. Syst. Meas. Control.* **2014**, *136*, 064504. [[CrossRef](#)]
8. Zhang, J.; Cheng, M.; Luo, X.; Li, H.; Luo, L.; Cheng, X.; Yan, X.; Shen, S. Current status of the research on key technologies of vehicle fuel cell stack. *J. Autom. Saf. Energy* **2022**, *13*, 1–28.
9. Hannan, M.A.; Azidin, F.; Mohamed, A. Multi-sources model and control algorithm of an energy management system for light electric vehicles. *Energy Convers. Manag.* **2012**, *62*, 123–130. [[CrossRef](#)]
10. Li, Q.; Yang, H.; Han, Y.; Li, M.; Chen, W. A state machine strategy based on droop control for an energy management system of PEMFC-battery-supercapacitor hybrid tramway. *Int. J. Hydrog. Energy* **2016**, *41*, 16148–16159. [[CrossRef](#)]
11. Zhao, Z.-H. Improved fuzzy logic control-based energy management strategy for hybrid power system of FC/PV/battery/SC on tourist ship. *Int. J. Hydrog. Energy* **2022**, *47*, 9719–9734. [[CrossRef](#)]
12. Hu, D.; Cheng, S.; Zhou, J.; Hu, L. Energy Management Optimization Method of Plug-In Hybrid-Electric Bus Based on Incremental Learning. *IEEE J. Emerg. Sel. Top. Power Electron.* **2021**, *11*, 7–18. [[CrossRef](#)]
13. Wu, P.; Partridge, J.; Bucknall, R. Cost-effective reinforcement learning energy management for plug-in hybrid fuel cell and battery ships. *Appl. Energy* **2020**, *275*, 115258. [[CrossRef](#)]
14. Wang, Y.; Jiao, X. Dual Heuristic Dynamic Programming Based Energy Management Control for Hybrid Electric Vehicles. *Energies* **2022**, *15*, 3235. [[CrossRef](#)]
15. Broatch, A.; Olmeda, P.; Plá, B.; Dreif, A. Novel Energy Management Control Strategy for Improving Efficiency in Hybrid Powertrains. *Energies* **2022**, *16*, 107. [[CrossRef](#)]
16. Xu, L.; Yang, F.; Li, J.; Ouyang, M.; Hua, J. Real time optimal energy management strategy targeting at minimizing daily operation cost for a plug-in fuel cell city bus. *Int. J. Hydrog. Energy* **2012**, *37*, 15380–15392. [[CrossRef](#)]
17. Yi, F.; Lu, D.; Wang, X.; Pan, C.; Tao, Y.; Zhou, J.; Zhao, C. Energy Management Strategy for Hybrid Energy Storage Electric Vehicles Based on Pontryagin’s Minimum Principle Considering Battery Degradation. *Sustainability* **2022**, *14*, 1214. [[CrossRef](#)]
18. Li, S.; Chu, L.; Hu, J.; Pu, S.; Li, J.; Hou, Z.; Sun, W. A Novel A-ECMS Energy Management Strategy Based on Dragonfly Algorithm for Plug-in FCEVs. *Sensors* **2023**, *23*, 1192. [[CrossRef](#)]
19. Pereira, D.F.; Lopes, F.D.C.; Watanabe, E.H. Nonlinear Model Predictive Control for the Energy Management of Fuel Cell Hybrid Electric Vehicles in Real Time. *IEEE Trans. Ind. Electron.* **2021**, *68*, 3213–3223. [[CrossRef](#)]
20. Moré, J.J.; Puleston, P.F.; Fossas, E.; Kunusch, C. Decoupled inputs sliding mode controllers for a fuel cell-supercapacitor module in hybrid generation applications. *Int. J. Energy Environ. Eng.* **2019**, *10*, 257–269. [[CrossRef](#)]
21. Zhou, D.; Al-Durra, A.; Matraji, I.; Ravey, A.; Gao, F. Online Energy Management Strategy of Fuel Cell Hybrid Electric Vehicles: A Fractional-Order Extremum Seeking Method. *IEEE Trans. Ind. Electron.* **2018**, *65*, 6787–6799. [[CrossRef](#)]
22. Zhao, D.; Gao, F.; Bouquain, D.; Dou, M.; Miraoui, A. Sliding-Mode Control of an Ultrahigh-Speed Centrifugal Compressor for the Air Management of Fuel-Cell Systems for Automotive Applications. *IEEE Trans. Veh. Technol.* **2013**, *63*, 51–61. [[CrossRef](#)]
23. Li, H.; Ravey, A.; N’diaye, A.; Djerdir, A. Online adaptive equivalent consumption minimization strategy for fuel cell hybrid electric vehicle considering power sources degradation. *Energy Convers. Manag.* **2019**, *192*, 133–149. [[CrossRef](#)]
24. Choi, E.; Kim, E. Critical aggressive acceleration values and models for fuel consumption when starting and driving a passenger car running on LPG. *Int. J. Sustain. Transp.* **2016**, *11*, 395–405. [[CrossRef](#)]
25. Zhou, M.; Jin, H.; Wang, W. A review of vehicle fuel consumption models to evaluate eco-driving and eco-routing. *Transp. Res. Part D Transp. Environ.* **2016**, *49*, 203–218. [[CrossRef](#)]
26. Tian, X.; Cai, Y.; Sun, X.; Zhu, Z.; Xu, Y. An adaptive ECMS with driving style recognition for energy optimization of parallel hybrid electric buses. *Energy* **2019**, *189*, 116151. [[CrossRef](#)]
27. Qin, D.; Zhan, S.; Zeng, Y.; Su, L. Management Strategy of Hybrid Electrical Vehicle Based on Driving Style Recognition. *J. Mech. Eng.* **2016**, *52*, 162–169. [[CrossRef](#)]
28. Guo, Q.; Zhao, Z.; Shen, P.; Zhan, X.; Li, J. Adaptive optimal control based on driving style recognition for plug-in hybrid electric vehicle. *Energy* **2019**, *186*, 115824. [[CrossRef](#)]

29. Murphey, Y.L.; Milton, R.; Kiliaris, L. Driver's style classification using jerk analysis. In Proceedings of the 2009 IEEE Workshop on Computational Intelligence in Vehicles and Vehicular Systems, Nashville, TN, USA, 30 March–2 April 2009; pp. 23–28.
30. Brombacher, P.; Masino, J.; Frey, M.; Gauterin, F. Driving event detection and driving style classification using artificial neural networks. In Proceedings of the 2017 IEEE International Conference on Industrial Technology (ICIT), Toronto, ON, Canada, 22–25 March 2017; pp. 997–1002. [[CrossRef](#)]
31. Zeng, T.; Zhang, C.; Zhang, Y.; Deng, C.; Hao, D.; Zhu, Z.; Ran, H.; Cao, D. Optimization-oriented adaptive equivalent consumption minimization strategy based on short-term demand power prediction for fuel cell hybrid vehicle. *Energy* **2021**, *227*, 120305. [[CrossRef](#)]
32. Li, H.; Ravey, A.; N'Diaye, A.; Djerdir, A. A novel equivalent consumption minimization strategy for hybrid electric vehicle powered by fuel cell, battery and supercapacitor. *J. Power Sources* **2018**, *395*, 262–270. [[CrossRef](#)]
33. Yue, M.; Jemei, S.; Gouriveau, R.; Zerhouni, N. Review on health-conscious energy management strategies for fuel cell hybrid electric vehicles: Degradation models and strategies. *Int. J. Hydrog. Energy* **2019**, *44*, 6844–6861. [[CrossRef](#)]
34. Guzzella, L.; Sciarretta, A. *Vehicle Propulsion Systems, Introduction to Modeling and Optimization*, 1st ed.; Springer: Berlin/Heidelberg, Germany, 2005.
35. Kim, J.; Kim, M.; Kang, T.; Sohn, Y.-J.; Song, T.; Choi, K.H. Degradation modeling and operational optimization for improving the lifetime of high-temperature PEM (proton exchange membrane) fuel cells. *Energy* **2014**, *66*, 41–49. [[CrossRef](#)]
36. Gao, F.; Blunier, B.; Miraoui, A. PEM Fuel Cell Stack Modeling for Real-Time Emulation in Hardware-in-the-Loop Applications. *IEEE Trans. Energy Convers.* **2010**, *26*, 184–194. [[CrossRef](#)]
37. Zheng, C.; Oh, C.; Park, Y.; Cha, S. Fuel economy evaluation of fuel cell hybrid vehicles based on equivalent fuel consumption. *Int. J. Hydrog. Energy* **2012**, *37*, 1790–1796. [[CrossRef](#)]
38. Zhou, Y.; Ravey, A.; Péra, M.-C. Real-time cost-minimization power-allocating strategy via model predictive control for fuel cell hybrid electric vehicles. *Energy Convers. Manag.* **2021**, *229*, 113721. [[CrossRef](#)]
39. Han, J.; Park, Y.; Kum, D. Optimal adaptation of equivalent factor of equivalent consumption minimization strategy for fuel cell hybrid electric vehicles under active state inequality constraints. *J. Power Sources* **2014**, *267*, 491–502. [[CrossRef](#)]
40. Kandidayeni, M.; Trovão, J.; Soleymani, M.; Boulon, L. Towards health-aware energy management strategies in fuel cell hybrid electric vehicles: A review. *Int. J. Hydrog. Energy* **2022**, *47*, 10021–10043. [[CrossRef](#)]
41. Pei, P.; Chang, Q.; Tang, T. A quick evaluating method for automotive fuel cell lifetime. *Int. J. Hydrog. Energy* **2008**, *33*, 3829–3836. [[CrossRef](#)]
42. Zhou, J.; Liu, J.; Xue, Y.; Liao, Y. Total travel costs minimization strategy of a dual-stack fuel cell logistics truck enhanced with artificial potential field and deep reinforcement learning. *Energy* **2021**, *239*, 121866. [[CrossRef](#)]
43. Shen, P.; Zhao, Z.; Li, J.; Zhan, X. Development of a typical driving cycle for an intra-city hybrid electric bus with a fixed route. *Transp. Res. Part D Transp. Environ.* **2018**, *59*, 346–360. [[CrossRef](#)]
44. Gong, Q.; Midlam-Mohler, S.; Marano, V.; Rizzoni, G. An Iterative Markov Chain Approach for Generating Vehicle Driving Cycles. *SAE Int. J. Engines* **2011**, *4*, 1035–1045. [[CrossRef](#)]
45. Xu, L.; Ouyang, M.; Li, J.; Yang, F.; Lu, L.; Hua, J. Application of Pontryagin's Minimal Principle to the energy management strategy of plugin fuel cell electric vehicles. *Int. J. Hydrog. Energy* **2013**, *38*, 10104–10115. [[CrossRef](#)]

**Disclaimer/Publisher's Note:** The statements, opinions and data contained in all publications are solely those of the individual author(s) and contributor(s) and not of MDPI and/or the editor(s). MDPI and/or the editor(s) disclaim responsibility for any injury to people or property resulting from any ideas, methods, instructions or products referred to in the content.